THE JOURNAL OF PHYSICAL CHEMISTRY LETTERS
A JOURNAL OF THE AMERICAN CHEMICAL SOCIETY

pubs.acs.org/JPCL Letter

Molecular Density Fluctuations Control Solubility and Diffusion for Confined Aqueous Hydrogen

Khang Quang Bui, Tran Thi Bao Le, Gabriel D. Barbosa, Dimitrios V. Papavassiliou, Sepideh Razavi, and Alberto Striolo*

Cite This: https://doi.org/10.1021/acs.jpclett.4c01684 Read Online

ACCESS | Metrics & More | Article Recommendations | Supporting Information

ABSTRACT: Hydrogen's contribution to a sustainable energy transition requires intermittent storage technologies, e.g., underground hydrogen storage (UHS). Toward designing UHS sites, atomistic molecular dynamics (MD) simulations are used here to quantify thermodynamic and transport properties for confined aqueous H_2. Slit-shaped pores of width 10 and 20 Å are carved out of kaolinite. Within these pores, water yields pronounced hydration layers. Molecular H_2 distributes along these hydration layers, yielding solubilities up to ∼25 times those in the bulk. Hydrogen accumulates near the siloxane surface, where water density fluctuates significantly. On the contrary, a dense hydration layer forms on the gibbsite surface, which is, for the most part, depleted of H_2. Although confinement reduces water mobility, the diffusion of aqueous H_2 increases as the kaolinite pore width decreases, a consequence of water density fluctuations. These results relate to H_2 permeability in underground hydrogen storage sites.

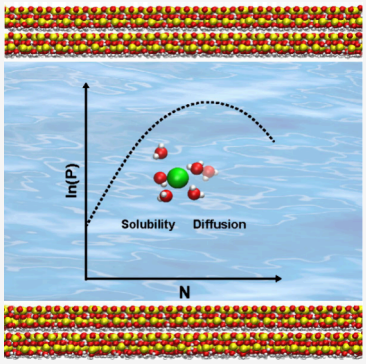

Currently, 70 million tons per annum of H_2 is produced globally[1] predominantly from natural gas and coal.[2] In the future, blue, green, and turquoise hydrogen[3] could help industry achieve ambitious decarbonization objectives,[4−6] provided novel methodologies are available for the intermittent storage of substantial quantities of this gas.[7] Traditionally, storing large amounts of hydrogen gas has proven to be challenging because of its low volumetric energy density,[8] high reactivity in the presence of oxygen, and potential high leakage rate, among other hurdles.[9] As a potential approach, large-scale underground hydrogen storage (UHS) might offer a more economical and safer technology compared to conventional surface storage technologies.[10,11] In addition to salt caverns, depleted underground reservoirs could serve as UHS sites due to their vast storage space, abundance across the US territory, and pre-existing infrastructure.[12,13] However, several fundamental questions need to be addressed. For example, because H_2 molecules are much smaller than hydrocarbon ones, and because they are likely to interact with other fluid components as well as with mineral surfaces, it is necessary to understand how confinement in the subsurface, where multiple fluids are present, including water and brines, affects thermodynamic and transport properties of H_2 gas. Indeed, a large body of literature shows that confinement affects the behavior of a variety of fluids.[14−16] The US Department of Energy's (DoE) National Hydrogen Storage Project boosted the development of novel materials for on-site reversible hydrogen storage and contributed to the transition to a hydrogen economy.[17−19] For example, prior studies show that adsorption in porous materials could increase H_2 density to 70.4 ($g_{H_2}\cdot L^{-1}$) for novel carbon−boron−nitrogen (CBN) heterocycle materials.[20] Only recently, the community has started to investigate the behavior of H_2 in confined water, with direct relevance to UHS.[15,21,22] In this regard, confinement in kaolinite clay is relevant, as this material is one of the most common minerals found in subsurface reservoirs.[23]

Hydrogen solubility and diffusivity in hydrated clay nanopores are expected to affect storage capacity and permeability in potential UHS sites. For example, H_2 dissolution in hydrated cap rocks could not only lead to leaks but also to undesired chemical reactions that compromise sealing capacity.[10,24] Water is ubiquitous in the subsurface, and in fact, it is frequently used to control hydrocarbon production. Although H_2 has low solubility in bulk water, confinement effects are likely to affect water structure and dynamics, potentially altering aqueous H_2 behavior. This hypothesis is supported by some recent experiments.[15,25−27] For instance, Firuznia et al.[15] reported a significant increase in hydrogen solubility in confined water when the pore size of zeolite is smaller than 2 nm; at those conditions, the orientation of water molecules was found, based on FT-IR experiments, to have a significant impact on H_2 uptake. NMR results from Miachon et al.[25] revealed a considerable increase in the solubility of H_2 in

Received: June 6, 2024
Revised: July 18, 2024
Accepted: July 19, 2024

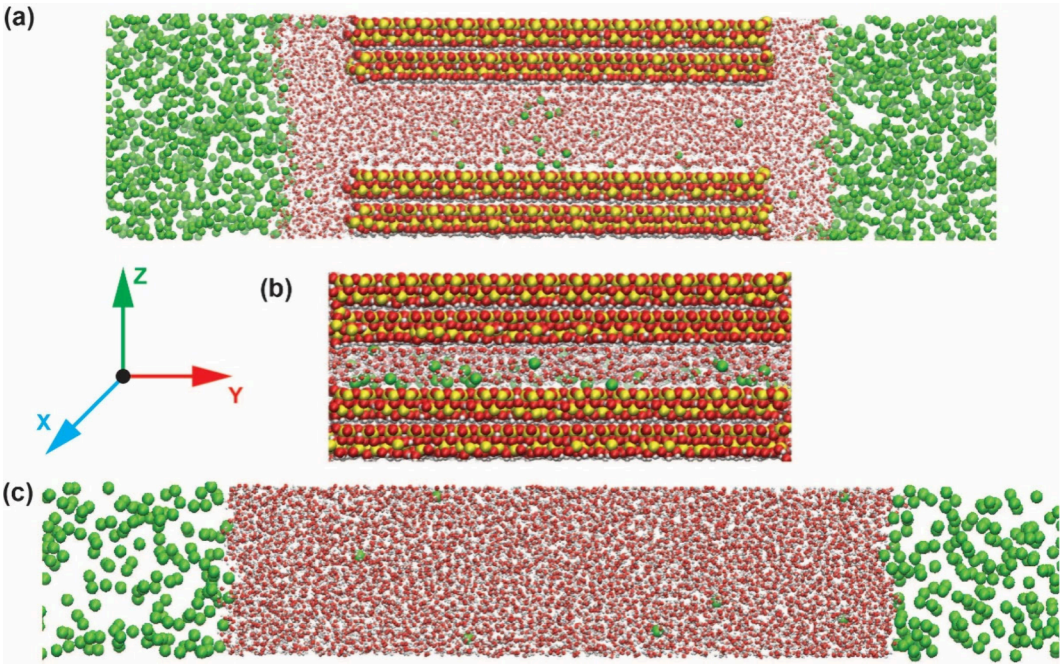

Figure 1. Schematic representation of the simulated systems. Panel (a) represents the system used to model the solubility of H_2 in confined water. Note that the water-filled pore is exposed to gaseous H_2. When equilibrium is reached and the number of H_2 molecules in the pore is constant, system (b) is used to model the diffusion coefficient for both water and H_2. In this system, the pore is effectively infinite along the *X* and *Y* directions. System (c) is used to obtain H_2 solubility in bulk water. The thickness of the water film is large enough to obtain bulk-like properties in its interior. Color code: Si, Al = yellow; O = red; H = white; H_2 = green. Water molecules are scaled down in size for better visualization.

γ-alumina nanopores. Wang et al.[26] found that the diffusivity of hydrogen in pulverized shale samples at 30 °C (i.e., 1.3×10^{-8} ($m^2 \cdot s^{-1}$)) was higher than that of methane. To generalize these practical observations, one must uncover the molecular mechanisms that control H_2 behavior in confined water, an exquisite fundamental quest.

Molecular simulations provide a powerful tool to interrogate confined systems.[15,22,28−31] For example, using Monte Carlo methods (MC), Zhang et al.[29] found that the H_2 loading density in 2 nm-wide pores filled with water was ∼3 times higher than the bulk solubility; this ratio can reach 27 in pores of width 0.55 nm. Yu et al.,[30] using molecular dynamics (MD), found that kaolinite nanopores could enhance the H_2 solubility in water up to 10 times compared to bulk values. However, the pores considered were confined by surfaces of identical hydrophilicity, which is not realistic.[32] The differences among these results suggest that both pore width and surface chemistry have a strong impact on H_2 solubility in confined water. To rationalize these observations, the molecular mechanisms responsible for the increased solubility, which currently remain unknown, need to be identified and understood. As for H_2 diffusivity, Liu et al.[22] reported that the H_2 diffusion coefficient in montmorillonite nanopores partially filled with water was $\sim 10^{-8}$ ($m^2 \cdot s^{-1}$), the value being significantly affected by temperature, pore size, and pressure. On the other hand, Choudhary et al.[31] recently reported a marked preference for clustering of CO_2 and H_2 within nanopores. In these systems, water forms well-formed layers,[21,22,33−35] which might lead to different H_2 behavior throughout the pore. To generalize the above observations concerning H_2 solubility and diffusivity in confined water, this work identifies and quantifies said variations from a molecular perspective.

In this letter, MD simulations were implemented to study H_2 solubility and diffusion behavior in water-filled kaolinite slit pores. The pore widths considered, 20 and 10 Å, allow us to test conditions at which the severity of confinement effects on water properties increases.[35−37] To maintain a realistic description of the clay system, the pore volume is confined by gibbsite and siloxane surface terminations; the former is considered hydrophilic, the latter hydrophobic.[38] As we discussed elsewhere,[39] in realistic systems most of the pore volume is likely to be found when gibbsite and siloxane basal surfaces face each other, which could occur when the clays expand as well as when kaolinite particles agglomerate. As such, edge effects are not considered explicitly herein. These effects are likely to affect the mechanisms of H_2 penetration and release from the slit-shaped pores. The model details are discussed in the Supporting Information section (SI). A visual for the simulated systems is displayed in Figure 1. The pressure was set at either 100 or 200 bar, relevant for UHS.[10] The temperature for all simulations was 298 K, slightly cooler than the reservoir temperature of 318 K.[40] The small temperature difference is not expected to alter the results significantly, while conducting the simulations at 298 K allows validation of the computational results with future experiments, conducted at ambient conditions.

As shown schematically in Figure S1, the solubility of hydrogen in water, *S*, can be obtained for both bulk and confined systems, as follows:

$$S = \frac{\rho_{H_2}}{\rho_{H_2O}} \quad (1)$$

In eq 1, ρ_{H_2}, and ρ_{H_2O} are the molar densities of hydrogen and water, respectively, in either the pores or in the bulk. The results, presented in Table 1, show that the H_2 solubility in

https://doi.org/10.1021/acs.jpclett.4c01684
J. Phys. Chem. Lett. XXXX, XXX, XXX−XXX

Table 1. Hydrogen Solubility in Water for Bulk and Confined Systems[a]

System	$S \times 10^3$
100 bar, bulk	1.41 ± 0.01
200 bar, bulk	2.81 ± 0.02
100 bar, 20 Å	3.55 ± 0.71
200 bar, 20 Å	7.34 ± 0.52
100 bar, 10 Å	36.01 ± 1.42
200 bar, 10 Å	35.50 ± 0.72

[a]In all cases, the temperature is 298 K. Confinement is provided by slit-shaped pores carved out of kaolinite.

bulk water at 100 and 200 bar is ∼1.41 × 10^{-3} and 2.81 × 10^{-3}, respectively. These values agree with experimental data reported by Wiebe et al.[41] Our results show that confinement notably enhances H_2 solubility in water, with variations due to both pressure and pore size. Although it has been reported for other gases that solubility in confined water changes with respect to bulk;[42−44] it is not always the case that confinement enhances solubility. Our results show that for a kaolinite pore of width 20 Å, the solubility at both 100 and 200 bar is ∼2.5 times that in bulk water. This ratio increases substantially in the smaller pore considered, for which H_2 solubility approaches 25 times that of the bulk. These results are consistent with those found for nonpolar gases, for which confinement is found to enhance solubility in water—an observation that led to the term "oversolubility".[15,25,29,45,46] Results for H_2 solubility in confined water seem to be consistent with these trends. Zhang et al.,[29] e.g., showed that as the pore width decreases from 2 to 0.55 nm, the H_2 solubility in confined water increases. As another example of nonpolar gas, Phan et al.[45] reported that confinement in silica slit-shaped nanopores could enhance the solubility of methane up to 50 times compared to that in the bulk. Luzar et al.[46] reported a significant increase in solubility for N_2, as well as for CO_2, in water due to hydrophobic confinement. On the other hand, the solubility of H_2 in confined water is affected by the chemistry of the confining materials.[28,30] For example, while Yu et al.[30] predicted a 10-fold enhancement of H_2 solubility in hydrated kaolinite pores, Ho et al.[28] did not observe H_2 oversolubility in nanopores carved out of montmorillonite. As an example for another gas, Li et al.[47] reported that CO_2 solubility in water decreases within hydrophilic kaolinite nanopores while it increases within hydrophobic pores. To generalize the results as a function of pore width and pore chemistry, Apostolopoulou et al.[48,49] showed that it is possible to employ a mesoscale approach based on kinetic Monte Carlo, once selected results from atomistic MD simulations are available.

However, the mechanism driving oversolubility remains under debate. Ho et al.[50] suggested that, in confinement, the density of octamethylcyclotetrasiloxane (OMCTS) is not uniform, allowing H_2 gas molecules to occupy regions of low OMCTS density. Meanwhile, CH_4 oversolubility was found to be driven by the strong interaction between the CH_4 molecules and the pore surface. However, Badmos et al.[37] reported that for H_2S molecules, the mechanism proposed by Ho et al.[50] was not applicable due to the lack of favorable adsorption of H_2S molecules close to the substrate surfaces. To identify the molecular mechanism responsible for the results observed herein, we start by analyzing the molecular density profiles within the pores.

Figure 2 shows the density profiles of water and H_2 along the direction perpendicular to the pore surface. Pronounced hydration layers are clearly visible. As seen in Figure 2a, the water density near the center of the 20-Å pore approaches that of bulk water, ∼33.332 (nm^{-3});[51] conversely, pronounced peaks are found in the middle of the 10-Å pore (Figure 2b), consistent with findings by Liu et al.,[22] focused on montmorillonite nanopores. Our results show that water

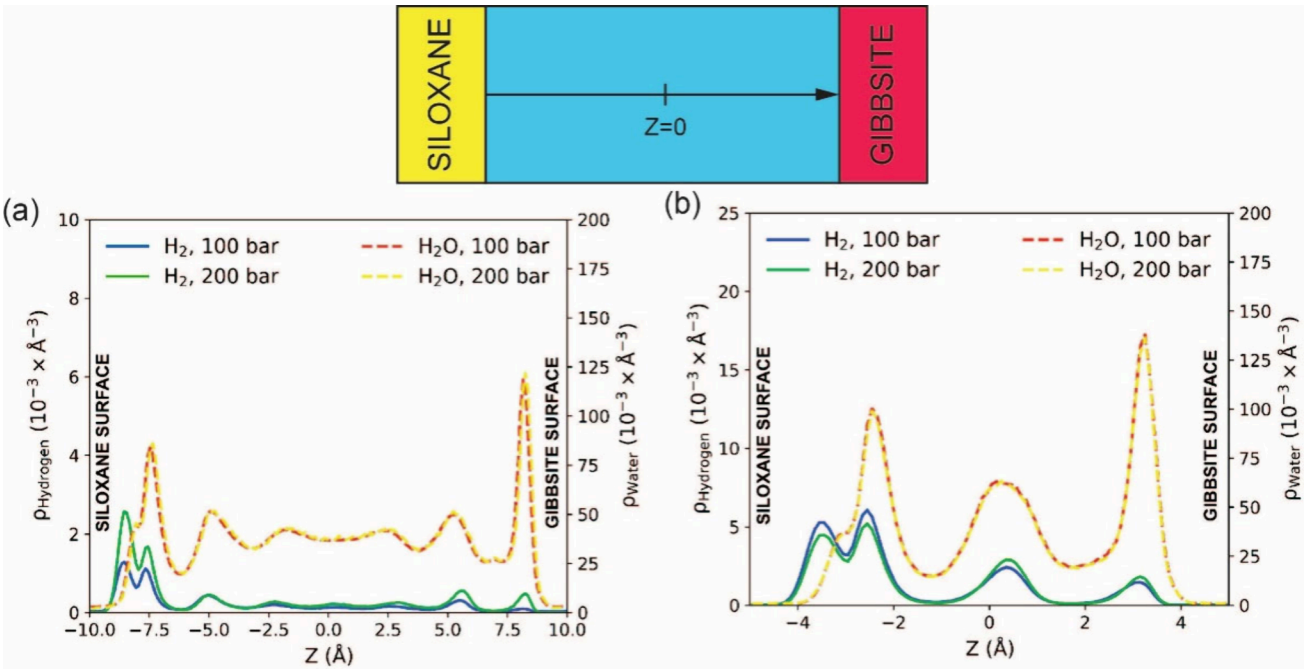

Figure 2. Atomic density profiles for H_2 molecules and water oxygen atoms along the direction perpendicular to the pore surface for different pore sizes: (a) 20 Å and (b) 10 Å. In both cases, the pore center is at $Z = 0$. The positions of the gibbsite and siloxane surfaces along the Z-direction are indicated on the plots. Only the pore volume is used for these calculations.

https://doi.org/10.1021/acs.jpclett.4c01684
J. Phys. Chem. Lett. XXXX, XXX, XXX−XXX

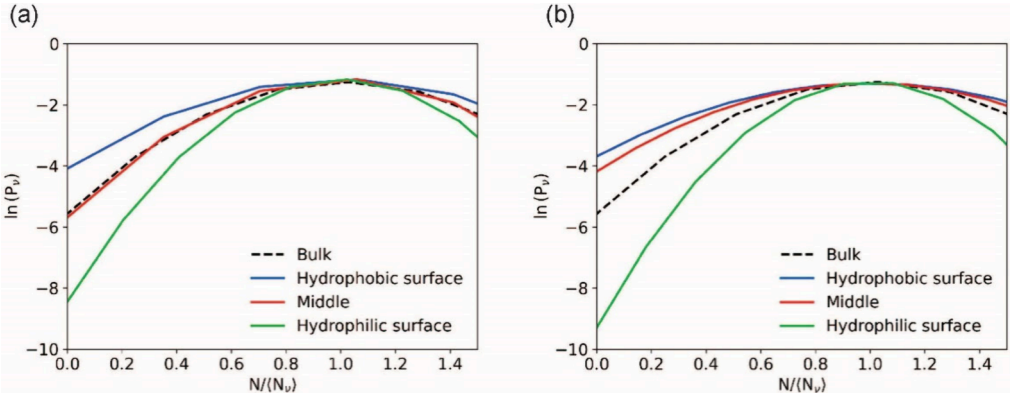

Figure 3. Probability of observing N water molecules, $P_\nu(N)$, in small volumes, ν, for pore sizes of (a) 20 Å and (b) 10 Å. The results were obtained from systems containing only water inside the kaolinite pores. For comparison, the results obtained for bulk water are shown as the dotted line in both panels. These simulations were conducted at 298 K and 100 bar.

accumulates near the gibbsite hydrophilic surface, where a more intense density peak is observed. In contrast, near the hydrophobic siloxane surface, a small shoulder is found in the density profile, whose peak has lower intensity than the one near the hydrophilic surface.

As shown in Figure 2, the distribution of hydrogen molecules across the hydrated kaolinite pores is strongly correlated with the water density distributions. In fact, H_2 accumulates near the siloxane surface, where water density is relatively low. This could lead to the question of whether hydrogen gas can dehydrate the hydrophobic kaolinite pores. Choudhary et al.[31] showed that even though the hydrophobic nanopore induces the formation of gas dimers or clusters the weak quadrupole moment of H_2 makes it less favorable to cluster formation compared to CO_2. In contrast, only a few H_2 molecules are found near the gibbsite surface, presumably because water molecules are highly packed in this hydration layer, leaving little room for guest gas. This behavior aligns with observations by Ho et al.,[50] who pointed out that H_2 accumulates in spaces with low solvent density. While the results just discussed hold true for both pores considered here, significant differences are noted concerning H_2 distribution near the center of the hydrated pores. Explicitly, the nearly negligible H_2 density in the middle of the 20-Å pore suggests minimal confinement effects, contrasting with the smaller pore, where abundant H_2 was found near the pore center. This unusual distribution can be explained by considering the mechanism of gas solubility, which consists of the formation of cavities where solute molecules can interact with the surrounding solvent.[52] For nonpolar gases like H_2, this mechanism is likely connected with molecular density fluctuations observed for water.[52,53] This mechanism has been invoked, e.g., to explain the increased solubility of CO_2 due to confinement.[54]

To test this possibility, a thorough evaluation of changes in water properties as a function of pore size is required. Hydrophobic effects, characterized by the inherent tendency of nonpolar solutes to either repel water molecules or exhibit mutual attraction within aqueous environments, have been studied previously.[55,56] Notably, Rego et al.[57] showed that higher degrees of hydrophobicity of a solute induce more intensive density fluctuations in the surrounding water. Building on this concept, we quantified water density fluctuations within the simulated pores. Hummer et al.[58] demonstrated that the probability distribution, $P_\nu(N)$, of observing N water molecules within a small, defined volume ν can be approximated by a Gaussian distribution function, as follows:

$$P_\nu(N) \approx \frac{1}{\sqrt{2\pi\sigma^2}} \exp\left[-\frac{(N - \langle N_\nu \rangle)^2}{2\sigma^2}\right] \quad (2)$$

In eq 2, $\langle N_\nu \rangle$ and σ are respectively the mean and variance of $P_\nu(N)$. Hummer et al. also indicated the relationship between the hydration free energy, G_{cav}, and $P_\nu(N)$:[58,59]

$$G_{cav} \approx \frac{k_B T}{2} \frac{\langle N_\nu \rangle^2}{\sigma^2} \quad (3)$$

These relations imply that enhanced water density fluctuations promote the formation of solute-size cavities, leading to increased solubility. To quantify water density fluctuations, identical virtual boxes were placed at three locations within the kaolinite pores: near the hydrophobic surface, near the middle of the pore, and near the hydrophilic surface. We minimized the size of the probe volumes ($4 \times 4 \times 3$ Å^3) while confirming that statistically meaningful results were achieved.

Figure 3 shows that $P_\nu(N)$ values near the siloxane surface are wider than those near the gibbsite one, indicating enhanced water density fluctuations near the siloxane surface.[60] As the pore width decreases (Figure 2b), the density fluctuations near the gibbsite surface become less probable, and those near the siloxane surface become more probable, suggesting that confinement enhances the wetting characteristics of each surface. Considering the probe volume located in the middle of the pore, the $P_\nu(N)$ distribution obtained within the 20-Å pore is somewhat comparable to that obtained for bulk water. On the contrary, when the pore width is 10 Å, the water density fluctuations extend to the middle of the pore. Garde et al.[59] indicated that enhanced water density fluctuations imply an increased propensity for cavity formation, thereby resulting in a diminished excess chemical potential for the solvation of hydrophobic solutes. Our results are consistent with this observation, as it is found that the H_2 solubility in confined water follows the trend: near siloxane surface > middle of the pore > near gibbsite surface. In addition, higher water density fluctuations near siloxane surface and in the middle of the 10-Å pore lead to higher solubility compared to results found in the larger pore considered. The density profiles shown in Figure 2

https://doi.org/10.1021/acs.jpclett.4c01684
J. Phys. Chem. Lett. XXXX, XXX, XXX−XXX

confirm that H_2 molecules can be found near the middle of the 10-Å pore, but not the 20-Å pore.

To illustrate the results discussed so far, in Figure 4 we report simulation snapshots for water and hydrogen molecules found within rectangular slabs of thickness ∼2 Å and parallel to the pore surfaces. From top to bottom, the results are for probe volumes near the hydrophilic surface, the middle of the pore, and the hydrophobic surface. For brevity, we only consider results obtained for the 10-Å pore. Left and right panels are for P = 100 and P = 200 bar, respectively. Results obtained for the 20-Å pore can be found in Figure S2 of the Supporting Information.

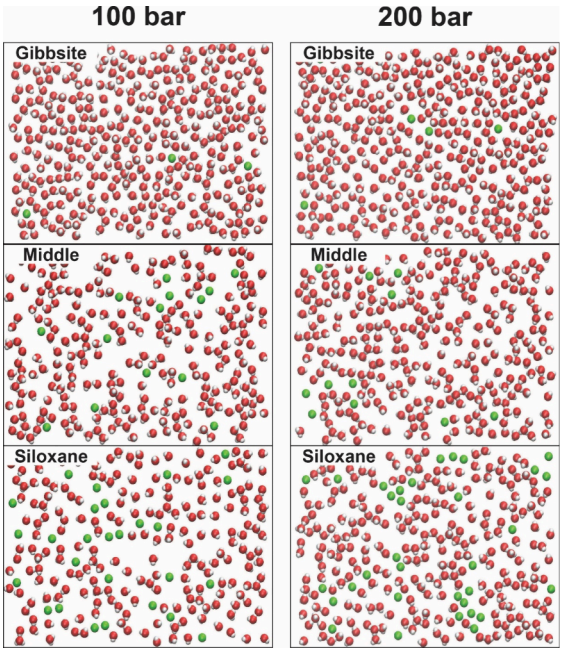

Figure 4. Top view simulation snapshots representing water and hydrogen molecules found within a probe volume of thickness of 10 Å located, from top to bottom, near the gibbsite, middle, and siloxane surface of the kaolinite pores, respectively. Left and right panels are obtained at P = 100 and P = 200 bar, respectively. In all cases, T = 298 K. Color code: O = red; H = white; H_2 = green.

The snapshots show that confinement affects the structure of water, with different results on the three layers considered. In the hydration layer near the gibbsite surface (top panels in Figure 4), a dense water layer is observed with few, if any, H_2 molecules, even at the largest pressure considered. Near the siloxane surface (bottom panels), the water structure is looser, allowing for more H_2 molecules to be present. In the middle layer it seems like the propensity of water molecules to hydrogen bond among themselves is combined with the appearance of cavities where H_2 molecules can aggregate, although individual hydrogen molecules can also be observed.

The results in Figure 4 confirm visually that confinement affects the structure of confined water, which in turn controls the solubility of aqueous hydrogen. Because the size of hydrogen molecules is smaller than that of water and because the enhanced solubility is found to be correlated with density fluctuations, it is of interest to quantify how the diffusivity of hydrogen gas in water changes with confinement. We start by computing the self-diffusion coefficient (D) via the Einstein's equation:[61]

$$D = \frac{1}{2d} \lim_{t\to\infty} \frac{d}{dt}\left[\left\langle \frac{1}{N}\sum_{i=1}^{N} |\mathbf{r}_d(t) - \mathbf{r}_d(t_0)|^2 \right\rangle\right] \quad (4)$$

In eq 4, d is the number of dimensions considered, $\mathbf{r}_d(t)$ and $\mathbf{r}_d(t_0)$ are the positions of atoms at time t and time t_0, respectively. The two-dimensional mean square displacement (MSD) (d = 2) was calculated for the confined systems, whereas the three-dimensional MSD (d = 3) was extracted for the simulated bulk systems. The MSD results obtained for water and H_2 in the kaolinite pores are shown in Figure 5. The MSD are calculated along the plane parallel to the solid substrate. The correspondent results for bulk systems are shown in Figure S3 of the Supporting Information. The results, in the form of self-diffusion coefficients, are summarized in Table 2. Of note, our bulk diffusion coefficients are comparable to literature experimental and simulation data.[62,63]

Visual inspection of the results in Figure 5 shows that while pressure has little effect on the MSD, the pore width has a strong impact on it. It is worth pointing out that the diffusion coefficients obtained for H_2 in the hydrated kaolinite pores are comparable to previous results obtained for C_3H_8, CH_4, H_2S, and CO_2.[34,35,37,64] Ghasemi et al.[21] reported H_2 diffusion in water-saturated slit pores at 300 bar in the range from 4.64×10^{-9} to 6.49×10^{-9} ($m^2 \cdot s^{-1}$) for modified montmorillonite and from 7.87×10^{-9} to 12.38×10^{-9} ($m^2 \cdot s^{-1}$) for modified beidellite clay substrates. These results confirm that both

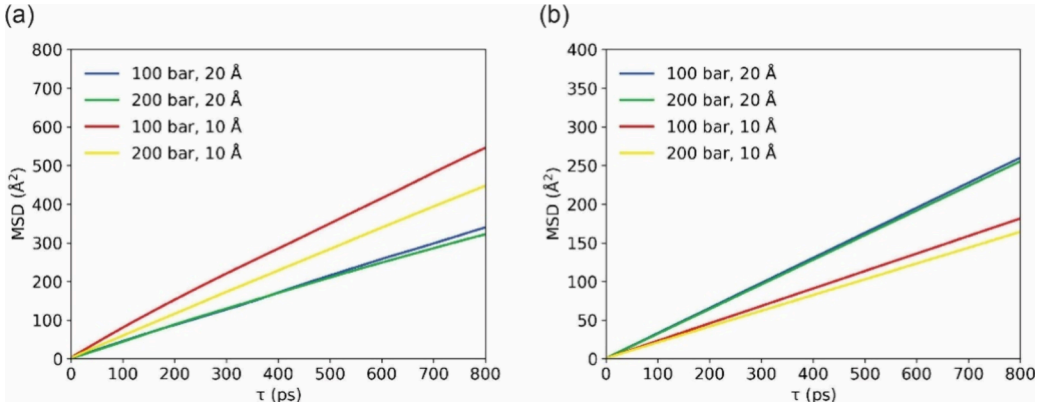

Figure 5. Two-dimensional mean square displacements (MSD) calculated for (a) hydrogen and (b) water confined in the kaolinite pores. Different colors represent different pores and different pressures. In all cases, T = 298 K.

https://doi.org/10.1021/acs.jpclett.4c01684
J. Phys. Chem. Lett. XXXX, XXX, XXX−XXX

Table 2. Diffusion Coefficients Computed for Hydrogen and Water Confined within Kaolinite Pores, Or in the Bulk, at 298 K and Different Pressures

System	Self-diffusion coefficients (10^{-10} $m^2 \cdot s^{-1}$)	
	Hydrogen	Water
100 bar, bulk	43.57 ± 1.40	26.07 ± 0.39
200 bar, bulk	68.55 ± 0.71	28.64 ± 0.81
100 bar, 20 Å	10.75 ± 0.51	08.07 ± 0.08
200 bar, 20 Å	10.32 ± 0.78	07.97 ± 0.04
100 bar, 10 Å	15.39 ± 0.22	05.72 ± 0.03
200 bar, 10 Å	13.84 ± 0.34	05.19 ± 0.08

confining material and pressure affect transport properties.[33,64] On the other hand, Liu et al.[22] reported that the H_2 diffusion coefficient in montmorillonite nanopores partially filled with water is ~4.25 × 10^{-8} ($m^2 \cdot s^{-1}$). This value is significantly higher than those obtained here, a difference explained by the fact that the pores were of width 3 nm, and only partially saturated with water. As water density increased, H_2 diffusion becomes slower.[22] As another reference point, Li et al.[47] reported diffusion coefficients ranging from 40 to 50 × 10^{-10} ($m^2 \cdot s^{-1}$) at 373 K and pressure up to 400 bar for CO_2 confined in kaolinite nanopores filled with water. These values are of the same order of magnitude as those obtained in this study.

The results in Table 2 show that reducing the pore width has different effects on the diffusivity of water and H_2. In the case of water, decreasing pore width reduces D, even though the results in Figure 3 show that reducing pore width increases water density fluctuations for the systems considered here. These results are consistent with literature observations.[35,65−68] Siboulet et al.,[65] e.g., demonstrated the strong impact of hydrophilic surfaces on the diffusion of confined water due to the strong water-substrate interactions. In addition, the reduced diffusion coefficients of water molecules can be attributed to their increased collision frequency under tight confinement.[66,67] The results obtained for H_2 differ substantially, as they show that reducing pore width increases diffusion. Indeed, at 100 bar, the H_2 diffusion coefficients in the 20 and 10 Å wide pores are 10.75 × 10^{-10} and 15.39 × 10^{-10} ($m^2 \cdot s^{-1}$), respectively. It is noteworthy that the D_{H_2}:D_{H_2O} ratio for the 20-Å pore is lower than that obtained in the bulk, while said ratio is significantly higher than in the bulk in the 10 Å pore.

To identify the mechanisms responsible for these observations, we refer to Phan et al.,[35] who showed that water structure and density fluctuations alter the diffusion mechanism for methane in hydrated nanopores. Because in the results above water density fluctuations were found to explain H_2 oversolubility in confined water, and because the increased diffusion coefficient of aqueous confined hydrogen seems to be uncorrelated with that of confined water, we suspect that the water density fluctuations are responsible for the enhanced diffusivity of confined aqueous H_2. To probe molecular differences between the transport of H_2 within the pores considered here, we compute the normalized velocity-velocity autocorrelation function (VACF) in the directions parallel to the pore surface, via:

$$C_{vv}(\tau) = \frac{\langle v(\tau) \cdot v(0) \rangle}{\langle v(0) \cdot v(0) \rangle} \quad (5)$$

In eq 5, $v(\tau)$ is the velocity of one hydrogen molecule at the time τ. The angular brackets indicate ensemble averages. The results are shown in Figure 6. All the curves are similar, with a

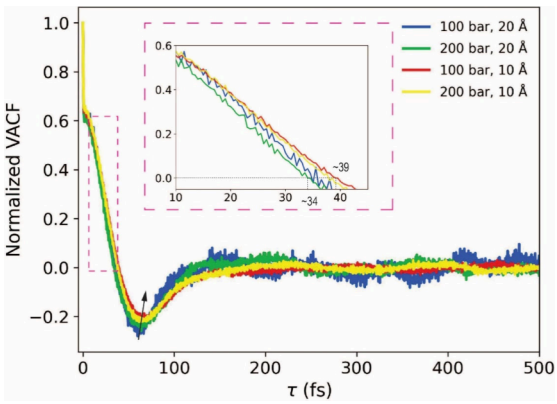

Figure 6. Normalized velocity autocorrelation function (VACF) of H_2 molecules in the hydrated pores at T = 298 K, P = 100, and 200 bar, and pore width 20 and 10 Å. Inset: Magnification (from 10 to 45 fs) shows the time τ that VACFs decay to 0.

quick decay in the first 100 fs, a pronounced minimum indicative of changes in direction, and oscillations around zero in the long time, before the curves decay to zero. These data are consistent with frequent collisions between hydrogen and water molecules within the pores.[69] It is notable that the results obtained in the 10-Å pore show longer characteristic times (the time at which the curves touch zero for the first time, the position of the minimum, and the long-time oscillations are all shifted to slightly longer times). These differences are consistent with H_2 molecules having access to more space for their motion in the smaller pore, confirming the impact of water density fluctuation on the diffusivity of confined aqueous H_2.

As the kaolinite surface is highly structured, we also investigated whether the diffusion of H_2 and water in kaolinite nanopores could be isotropic. The results, together with the projections of molecular trajectories for representative H_2 and H_2O molecules, are displayed in Figure S4 of the Supporting Information. Our observations suggest that, while water diffusion is isotropic, that of H_2 is somewhat anisotropic. This confirms that the behavior of aqueous H_2 is correlated with that of confined water.

To further probe the dynamics features of the confined H_2−H_2O system, we quantified the residence time for H_2 molecules in the various hydration layers via the algorithm introduced by Liu et al.[70] and described previously:[64,71]

$$P(\tau) = \frac{1}{K} \sum_{t=1}^{K} \frac{N(t, t+\tau)}{N(t)} \quad (6)$$

In eq 6, $P(\tau)$ is the probability for H_2 to remain in the interested region, K is the total number of origins averaged over, $N(t,t+\tau)$ and $N(t)$ are the number of hydrogen molecules in that region at the time $t+\tau$ and t. We considered regions near the siloxane surface, near the middle of the pores, and near the gibbsite surface, as identified by the water density profiles. The three layers were denoted as Layers I, II, and III, respectively. The volume of each layer was 52.5 × 48.5 × 2 ($Å^3$), as shown in Figure S5 of the SI. Our results are shown in Figure 7. To interpret these data, it helps remembering that the

https://doi.org/10.1021/acs.jpclett.4c01684
J. Phys. Chem. Lett. XXXX, XXX, XXX−XXX

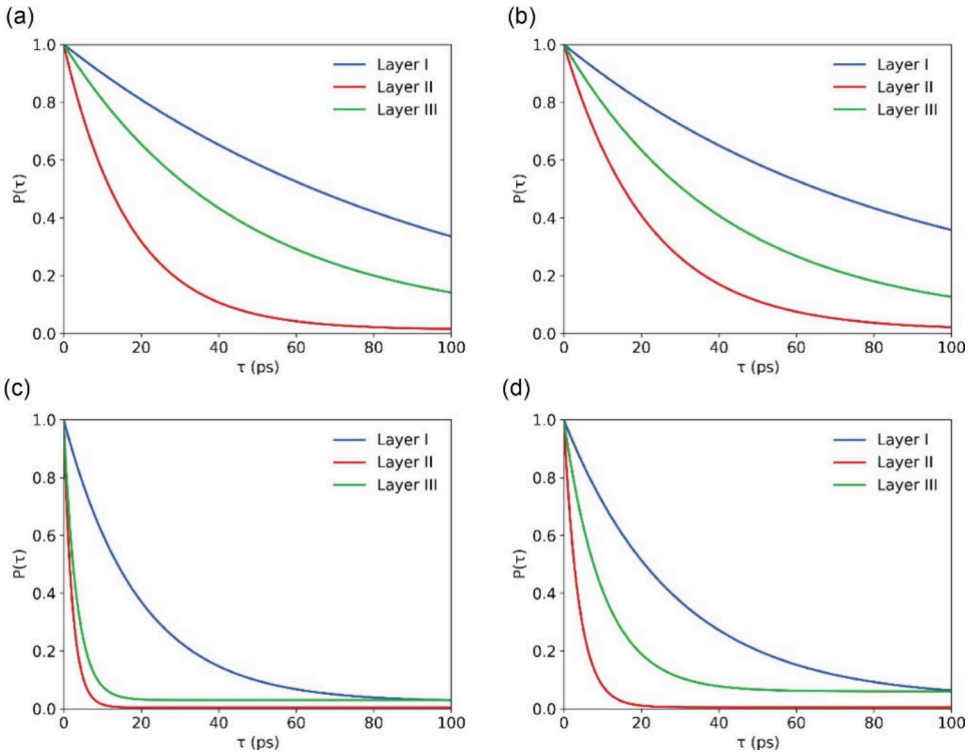

Figure 7. Residence probability of H_2 in different hydration layers for pressures and pore sizes of: (a) 100 bar, 20 Å; (b) 200 bar, 20 Å; (c) 100 bar, 10 Å; and (d) 200 bar, 10 Å. Layers I, II, and III are located near the siloxane surface, the middle of the pores, and the gibbsite surface, respectively. The volume of the probe volumes is constant, for consistency.

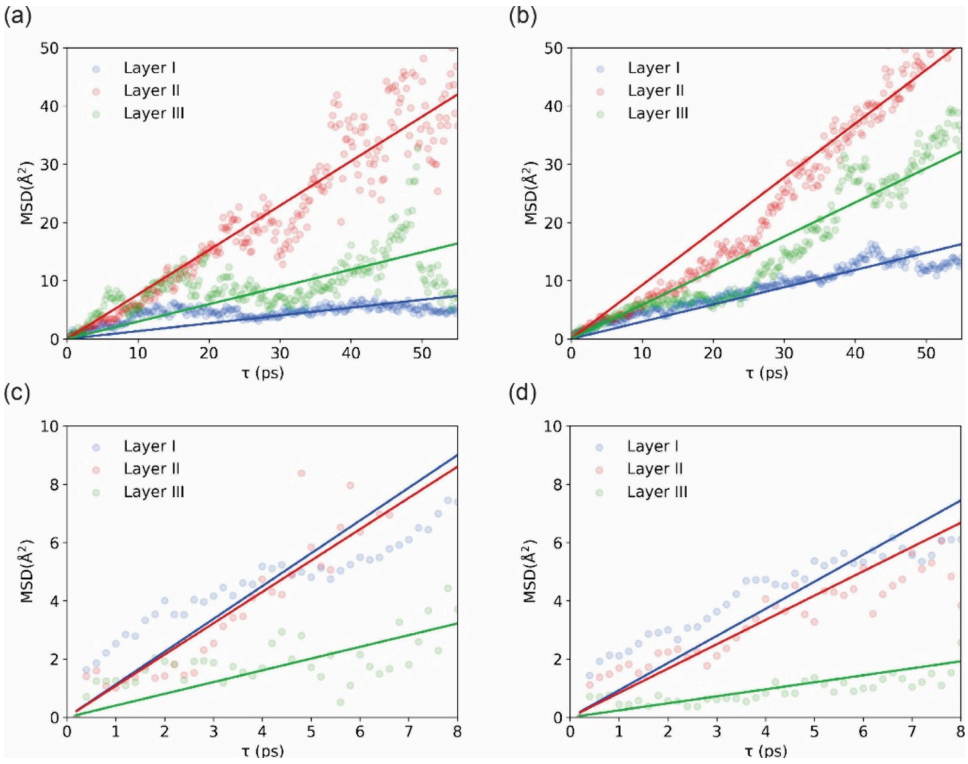

Figure 8. MSD for H_2 molecules found within different hydration layers located within kaolinite pores. Different panels are for different pore widths and different pressures: (a) 100 bar, 20 Å; (b) 200 bar, 20 Å; (c) 100 bar, 10 Å; and (d) 200 bar, 10 Å. In all cases, T = 298 K. Layers I, II, and III are located near the siloxane, middle, and gibbsite surfaces, respectively.

faster the decay of the probability $P(\tau)$, the faster H_2 molecules leave that layer. The results in both pores show a similar order of decay rate: Layer II > Layer III > Layer I, although the residence time is significantly longer in the 20-Å than in the 10-Å pore. In both pores, and at all pressures considered, the highest decay rate is observed in Layer II (middle of the pore),

https://doi.org/10.1021/acs.jpclett.4c01684
J. Phys. Chem. Lett. XXXX, XXX, XXX−XXX

suggesting that this region functions as a transition layer for confined aqueous H_2. Out of the other two hydration layers, the decay rate is faster near the gibbsite surface, where the hydration layer is dense and water density fluctuations are lower, than near the siloxane surface. These results suggest an anticorrelation between density fluctuations and residence time for H_2. This relation holds, however, only within a single pore.

Access to the data in Figure 7 allows us to compute the MSD for H_2 molecules as a function of their location within the hydrated pores, via the following equation:[70]

$$\langle \Delta r^2(t) \rangle_{\{a,b\}} = \frac{\left\langle \sum_{i \in \{a,b\}} |\mathbf{r}_i(t) - \mathbf{r}_i(0)|^2 \right\rangle}{N(0) \cdot P(t)} \tag{7}$$

In eq 7, $\langle \Delta r^2(t) \rangle_{\{a,b\}}$ represents the in-plane MSD of H_2 in layer {a,b}; $\mathbf{r}_i(t)$ and $\mathbf{r}_i(0)$ are the H_2 positions at time t and time t = 0; N(0) indicates the number of H_2 molecules present within the layer at the time t = 0; to account for the fact that the H_2 molecules in a hydration layer diffuse to other layers, P(t) is the residence probability from Figure 7. When a H_2 molecule leaves the region of interest, its displacement stops contributing to the MSD. To maintain reasonable statistical accuracy, the results, shown in Figure 8, were obtained for P(t) > 0.05.[71] It is worth noting that the resultant MSD profiles are only indicative.[72] Nevertheless, the observations are qualitatively important. In particular, the results show that in the 20-Å pore, H_2 transport is slowest near the siloxane surface, where the density profiles of Figure 2 indicate that aqueous H_2 accumulates in this pore. On the other hand, the results in Figure 8 show that within the 10-Å pore, H_2 diffusion is faster near the siloxane and near the middle of the pore, where most of the H_2 accumulates (see Figure 2). This observation explains why H_2 diffusion is faster in the narrower pore, where water diffusion is the slowest.

In summary, molecular dynamics simulations were used to discover the molecular mechanisms responsible for controlling solubility and diffusion of hydrogen gas within hydrated kaolinite nanopores. The results demonstrate a remarkable enhancement in hydrogen solubility, reaching up to 25 times that in bulk water in the narrower pore considered here (10 Å). The density profiles computed along the direction perpendicular to the solid surfaces revealed pronounced hydration layers, which extended across the entire pore for the narrower pore considered (10 Å). Hydrogen molecules show a strong preference for accumulating with respect to the position of the hydration layers. These correlations were explained by water density fluctuations. Because in the 10-Å pore, significant density fluctuations are observed for water even in the middle of the pore, hydrogen solubility in confined water is significantly increased compared not only to that in the bulk but also to that observed in the 20-Å pore. Confinement is also found to affect transport properties. In particular, while water diffusion is hindered by confinement, H_2 diffusion is enhanced. Detailed data analysis, including residence probability distributions, velocity−velocity autocorrelation functions, and estimations of the H_2 mobility within different hydration layers, illustrated a pronounced heterogeneous behavior for aqueous H_2 as a function of the pore width. These results support the conclusion that water density fluctuations, which depend on pore surface chemistry and pore width, indirectly affect the properties of aqueous H_2, thereby offering a tool for generalizing and predicting the behavior of H_2 in porous matrixes filled with water. Because such behavior controls the permeability of H_2, the results presented here are critical for the design of underground hydrogen storage facilities, in particular for preventing leaks. To extrapolate the results presented here to kaolinite pores of various widths, mesoscale approaches such as those based on kinetic Monte Carlo simulations are recommended.

■ METHODOLOGY

The MD simulations were implemented using the Large-scale Atomic/Molecular Massively Parallel Simulator (LAMMPS) program[73] (version second Aug 2023). The Verlet algorithm was applied to solve Newton's equations of motion with the time step of 1.0 fs.[74] The temperature and pressure of the simulation systems were controlled by the Nose-Hoover thermostat[75,76] and barostat.[77] The SHAKE constraint algorithm[78] was used to keep the bond and the angle of water molecules fixed. After energy minimization, the system was initially relaxed with 5 ns running in the canonical ensemble NVT (constant number of particles, volume, and temperature). Subsequently, the system was equilibrated by 20 ns run in the isothermal−isobaric NPT ensemble (constant number of particles, pressure, and temperature) followed by another 20 ns of NVT run. After that, 20 ns of NVT run was applied to equilibrate simulation systems. The equilibrium was determined by the following observations: The temperature and pressure of the system were stable, the density of hydrogen and water in the bulk were comparable to thermodynamic data from the National Institute of Standards and Technology (NIST),[79] the number of hydrogen molecules inside the pore remained constant for 2 ns. Three production runs were performed in the NVT ensemble for 5 ns. The coordinates of the various molecules were recorded every 200 ps of simulations. After that, the fully periodic confinement systems were obtained by carefully removing water and hydrogen in the bulk region. Then, they were relaxed for 15 ns, followed by three production runs of 5 ns, recorded every 200 fs, in the NVT ensemble. The system setups are discussed with more details in SI.

Regarding the force fields, the CLAYFF[80] and the Extended Simple Point Charge (SPC/E)[81] were used for the kaolinite substrates and water molecules, respectively. The recently developed CLAYFF force field,[82] which is able to describe pore edges, was not implemented here because the behavior of water and hydrogen near pore entrances was not studied. For H_2, several models have been developed over the past decades. These include single-site models,[83−85] two-site models,[86] two-site with quadrupole moment models,[87−89] and three-site with quadrupole moment.[90,91] In this study, the single-site Buch model[83] was applied because Tsimpanogiannis et al.[62] reported that it performs well in predicting several thermodynamic and transport properties. Azeezat et al.[92] conducted a performance comparison between the Buch model and the Marx force field in their ability to describe H_2. The findings indicated that the Buch model effectively characterized contact angles and gas−liquid interfacial tensions with the SPC/E water model and brought hydrogen density closer to experimental data. Moreover, implementing this single-site model has the added benefit of reducing simulation costs.[92,93] The force field parameters in this study are displayed in Table S1.

https://doi.org/10.1021/acs.jpclett.4c01684
J. Phys. Chem. Lett. XXXX, XXX, XXX−XXX

■ ASSOCIATED CONTENT

Supporting Information

The Supporting Information is available free of charge at https://pubs.acs.org/doi/10.1021/acs.jpclett.4c01684.

Details of simulation setup; force field parameters; atomic density profiles along the *Y*-direction; top view simulation snapshots representing water and hydrogen molecules found within a probe volume of thickness of 20 Å; MSD for hydrogen and water molecules in the bulk; diffusion coefficients in the *X*−*Y* plane and in *X* and *Y* directions of H_2 and H_2O and projection of trajectories of one representative H_2 and H_2O molecule for different conditions of pressures and pore sizes; and schematic representation for Layer I, Layer II, and Layer III (PDF)

■ AUTHOR INFORMATION

Corresponding Author

Alberto Striolo − *School of Sustainable Chemical, Biological, and Materials Engineering, The University of Oklahoma, Norman, Oklahoma 73019, United States;* orcid.org/0000-0001-6542-8065; Email: astriolo@ou.edu

Authors

Khang Quang Bui − *School of Sustainable Chemical, Biological, and Materials Engineering, The University of Oklahoma, Norman, Oklahoma 73019, United States*

Tran Thi Bao Le − *School of Sustainable Chemical, Biological, and Materials Engineering, The University of Oklahoma, Norman, Oklahoma 73019, United States*

Gabriel D. Barbosa − *School of Sustainable Chemical, Biological, and Materials Engineering, The University of Oklahoma, Norman, Oklahoma 73019, United States*

Dimitrios V. Papavassiliou − *School of Sustainable Chemical, Biological, and Materials Engineering, The University of Oklahoma, Norman, Oklahoma 73019, United States;* orcid.org/0000-0002-4583-0820

Sepideh Razavi − *School of Sustainable Chemical, Biological, and Materials Engineering, The University of Oklahoma, Norman, Oklahoma 73019, United States;* orcid.org/0000-0003-1225-6081

Complete contact information is available at: https://pubs.acs.org/10.1021/acs.jpclett.4c01684

Notes

The authors declare no competing financial interest.

■ ACKNOWLEDGMENTS

The authors acknowledge generous allocations of computing resources from the OU Supercomputing Center for Education & Research (OSCER) at the University of Oklahoma, Norman, Oklahoma, U.S.A., and from the Stampede3 at Texas Advanced Computing Center, through allocation TG-CHM240008 from the Advanced Cyberinfrastructure Coordination Ecosystem: Services & Support (ACCESS) program, which is supported by National Science Foundation grants #2138259, #2138286, #2138307, #2137603, and #2138296. K.Q.B. appreciates insightful assistance from Dr. Anh Phan, School of Chemistry and Chemical Engineering, Faculty of Engineering and Physical Sciences, University of Surrey, Guildford, Surrey GU2 7XH, United Kingdom, and from Dr. Felipe Perez, School of Sustainable Chemical, Biological and Materials Engineering, University of Oklahoma, Norman, Oklahoma 73019, United States. A.S. acknowledges support from the Asahi Glass Chair of Chemical Engineering at the University of Oklahoma. This work was supported, in part, by the US National Science Foundation under grant number 2317726.

■ REFERENCES

(1) Kazi, M.-K.; Eljack, F.; El-Halwagi, M. M.; Haouari, M. Green Hydrogen for Industrial Sector Decarbonization: Costs and Impacts on Hydrogen Economy in Qatar. *Comput. Chem. Eng.* **2021**, *145*, 107144.

(2) Dawood, F.; Anda, M.; Shafiullah, G. M. Hydrogen Production for Energy: An Overview. *Int. J. Hydrogen Energy* **2020**, *45* (7), 3847−3869.

(3) Yu, M.; Wang, K.; Vredenburg, H. Insights into Low-Carbon Hydrogen Production Methods: Green, Blue and Aqua Hydrogen. *Int. J. Hydrogen Energy* **2021**, *46* (41), 21261−21273.

(4) AlHumaidan, F. S.; Absi Halabi, M.; Rana, M. S.; Vinoba, M. Blue Hydrogen: Current Status and Future Technologies. *Energy Conversion and Management* **2023**, *283*, 116840.

(5) Lagioia, G.; Spinelli, M. P.; Amicarelli, V. Blue and Green Hydrogen Energy to Meet European Union Decarbonisation Objectives. An Overview of Perspectives and the Current State of Affairs. *Int. J. Hydrogen Energy* **2023**, *48* (4), 1304−1322.

(6) Bui, T.; Frampton, H.; Huang, S.; Collins, I. R.; Striolo, A.; Michaelides, A. Water/Oil Interfacial Tension Reduction − an Interfacial Entropy Driven Process. *Phys. Chem. Chem. Phys.* **2021**, *23* (44), 25075−25085.

(7) Noussan, M.; Raimondi, P. P.; Scita, R.; Hafner, M. The Role of Green and Blue Hydrogen in the Energy Transition - a Technological and Geopolitical Perspective. *Sustainability* **2021**, *13* (1), 298.

(8) Al-Yaseri, A.; Esteban, L.; Yekeen, N.; Giwelli, A.; Sarout, J.; Sarmadivaleh, M. The Effect of Clay on Initial and Residual Saturation of Hydrogen in Clay-Rich Sandstone Formation: Implications for Underground Hydrogen Storage. *Int. J. Hydrogen Energy* **2023**, *48* (13), 5175−5185.

(9) Hassanpouryouzband, A.; Joonaki, E.; Edlmann, K.; Haszeldine, R. S. Offshore Geological Storage of Hydrogen: Is This Our Best Option to Achieve Net-Zero? *ACS Energy Lett.* **2021**, *6* (6), 2181−2186.

(10) Zivar, D.; Kumar, S.; Foroozesh, J. Underground Hydrogen Storage: A Comprehensive Review. *Int. J. Hydrogen Energy* **2021**, *46* (45), 23436−23462.

(11) Patanwar, Y. K.; Kim, H.-M.; Deb, D.; Gujjala, Y. K. Underground Storage of Hydrogen in Lined Rock Caverns: An Overview of Key Components and Hydrogen Embrittlement Challenges. *Int. J. Hydrogen Energy* **2024**, *50*, 116−133.

(12) Sambo, C.; Dudun, A.; Samuel, S. A.; Esenenjor, P.; Muhammed, N. S.; Haq, B. A Review on Worldwide Underground Hydrogen Storage Operating and Potential Fields. *Int. J. Hydrogen Energy* **2022**, *47* (54), 22840−22880.

(13) Muhammed, N. S.; Haq, M. B.; Al Shehri, D. A.; Al-Ahmed, A.; Rahman, M. M.; Zaman, E.; Iglauer, S. Hydrogen Storage in Depleted Gas Reservoirs: A Comprehensive Review. *Fuel* **2023**, *337*, 127032.

(14) Chakraborty, S.; Kumar, H.; Dasgupta, C.; Maiti, P. K. Confined Water: Structure, Dynamics, and Thermodynamics. *Acc. Chem. Res.* **2017**, *50* (9), 2139−2146.

(15) Firuznia, R.; Jahanbakhsh, A.; Nazifi, S.; Ghasemi, H. Hydrogen Solubility in Confined Water. *Langmuir* **2024**, *40* (9), 4702−4708.

(16) Knight, A. W.; Kalugin, N. G.; Coker, E.; Ilgen, A. G. Water Properties under Nano-Scale Confinement. *Sci. Rep.* **2019**, *9* (1), 8246.

(17) None, N. *2010 Annual Progress Report Doe Hydrogen Program*; EERE Publication and Product Library: Washington, DC (United States), 2011.

(18) Satyapal, S.; Petrovic, J.; Read, C.; Thomas, G.; Ordaz, G. The U.S. Department of Energy's National Hydrogen Storage Project:

Progress Towards Meeting Hydrogen-Powered Vehicle Requirements. *Catal. Today* **2007**, *120* (3), 246−256.

(19) Klebanoff, L. E.; Keller, J. O. 5 years of Hydrogen Storage Research in the U.S. Doe Metal Hydride Center of Excellence (Mhcoe). *Int. J. Hydrogen Energy* **2013**, *38* (11), 4533−4576.

(20) Liu, S.-Y. *Hydrogen Storage by Novel Cbn Heterocycle Materials*; Univ. of Oregon: Eugene, OR (United States), 2015.

(21) Ghasemi, M.; Omrani, S.; Mahmoodpour, S.; Zhou, T. Molecular Dynamics Simulation of Hydrogen Diffusion in Water-Saturated Clay Minerals; Implications for Underground Hydrogen Storage (Uhs). *Int. J. Hydrogen Energy* **2022**, *47* (59), 24871−24885.

(22) Liu, J.; Wang, S.; Javadpour, F.; Feng, Q.; Cha, L. Hydrogen Diffusion in Clay Slit: Implications for the Geological Storage. *Energy Fuels* **2022**, *36* (14), 7651−7660.

(23) Detellier, C. Functional Kaolinite. *Chem. Rec.* **2018**, *18* (7−8), 868−877.

(24) Hagemann, B.; Rasoulzadeh, M.; Panfilov, M.; Ganzer, L.; Reitenbach, V. Hydrogenization of Underground Storage of Natural Gas. *Computational Geosciences* **2016**, *20* (3), 595−606.

(25) Miachon, S.; Syakaev, V. V.; Rakhmatullin, A.; Pera-Titus, M.; Caldarelli, S.; Dalmon, J.-A. Higher Gas Solubility in Nanoliquids? *ChemPhysChem* **2008**, *9* (1), 78.

(26) Wang, C.; Zhao, Y.; Wu, R.; Bi, J.; Zhang, K. Shale Reservoir Storage of Hydrogen: Adsorption and Diffusion on Shale. *Fuel* **2024**, *357*, 129919.

(27) Didier, M.. *Study of Reactive Transfer of Hydrogen within Intact Clay-Rock*; Grenoble Univ. (France), 2012.

(28) Ho, T. A.; Jove-Colon, C. F.; Wang, Y. Low Hydrogen Solubility in Clay Interlayers Limits Gas Loss in Hydrogen Geological Storage. *Sustainable Energy & Fuels* **2023**, *7* (14), 3232−3238.

(29) Zhang, H.; Luo, X.; Yang, D.; Liu, K.; Xie, Q.; Diao, R. Molecular Simulation of H2 Loss by Dissolution in Caprock Water-Saturated Nanopores under the Nanoconfinement Effect for Underground Hydrogen Storage. *Energy Fuels* **2023**, *37* (23), 19357−19368.

(30) Yu, S.; Zheng, R.; Kang, Q.; Mehana, M. Predicted Tenfold Increase of Hydrogen Solubility in Water under Pore Confinement. *Environmental Chemistry Letters* **2024**, *22* (3), 945−951.

(31) Choudhary, A.; Ho, T. A. Confinement-Induced Clustering of H2 and Co2 Gas Molecules in Hydrated Nanopores. *Phys. Chem. Chem. Phys.* **2024**, *26* (14), 10506−10514.

(32) Shang, Z.; Yang, Y.; Zhang, L.; Sun, H.; Zhong, J.; Zhang, K.; Yao, J. Hydrogen Adsorption and Diffusion Behavior in Kaolinite Slit for Underground Hydrogen Storage: A Hybrid Gcmc-Md Simulation Study. *Chem. Eng. J.* **2024**, *487*, 150517.

(33) Bui, T.; Phan, A.; Cole, D. R.; Striolo, A. Transport Mechanism of Guest Methane in Water-Filled Nanopores. *J. Phys. Chem. C* **2017**, *121* (29), 15675−15686.

(34) Ali, A.; Striolo, A.; Cole, D. R. Co2 Solubility in Aqueous Electrolyte Solutions Confined in Calcite Nanopores. *J. Phys. Chem. C* **2021**, *125* (22), 12333−12341.

(35) Phan, A.; Cole, D. R.; Striolo, A. Factors Governing the Behaviour of Aqueous Methane in Narrow Pores. *Philosophical Transactions of the Royal Society A: Mathematical, Physical and Engineering Sciences* **2016**, *374* (2060), 20150019.

(36) Le, T.; Striolo, A.; Cole, D. R. Co2−C4h10 Mixtures Simulated in Silica Slit Pores: Relation between Structure and Dynamics. *J. Phys. Chem. C* **2015**, *119* (27), 15274−15284.

(37) Badmos, S. B.; Striolo, A.; Cole, D. R. Aqueous Hydrogen Sulfide in Slit-Shaped Silica Nanopores: Confinement Effects on Solubility, Structural, and Dynamical Properties. *J. Phys. Chem. C* **2018**, *122* (26), 14744−14755.

(38) Le, T. T. B.; Finney, A. R.; Zen, A.; Bui, T.; Tay, W. J.; Chellappah, K.; Salvalaglio, M.; Michaelides, A.; Striolo, A. Mesoscale Simulations Reveal How Salt Influences Clay Particles Agglomeration in Aqueous Dispersions. *J. Chem. Theory Comput.* **2024**, *20* (4), 1612−1624.

(39) Zen, A.; Bui, T.; Bao Le, T. T.; Tay, W. J.; Chellappah, K.; Collins, I. R.; Rickman, R. D.; Striolo, A.; Michaelides, A. Long-Range Ionic and Short-Range Hydration Effects Govern Strongly Anisotropic Clay Nanoparticle Interactions. *J. Phys. Chem. C* **2022**, *126* (18), 8143−8151.

(40) Kanaani, M.; Sedaee, B. Impact of Dilation and Irreversible Compaction on Underground Hydrogen Storage in Depleted Hydrocarbon Reservoirs. *Energy Fuels* **2022**, *36* (22), 13506−13517.

(41) Wiebe, R. Solubility of Hydrogen in Water at 250c from 25 to 1000 atm. *Industrial & Engineering Chemistry* **1932**, *24* (7), 823−825.

(42) Campos, M. D.; Akkutlu, I. Y.; Sigal, R. F. A Molecular Dynamics Study on Natural Gas Solubility Enhancement in Water Confined to Small Pores. *Proceedings - SPE Annual Technical Conference and Exhibition* **2009**, DOI: 10.2118/124491-MS.

(43) Ho, L. N.; Schuurman, Y.; Farrusseng, D.; Coasne, B. Solubility of Gases in Water Confined in Nanoporous Materials: Zsm-5, Mcm-41, and Mil-100. *J. Phys. Chem. C* **2015**, *119* (37), 21547−21554.

(44) Breynaert, E.; Houlleberghs, M.; Radhakrishnan, S.; Grübel, G.; Taulelle, F.; Martens, J. A. Water as a Tuneable Solvent: A Perspective. *Chem. Soc. Rev.* **2020**, *49* (9), 2557−2569.

(45) Phan, A.; Cole, D. R.; Striolo, A. Aqueous Methane in Slit-Shaped Silica Nanopores: High Solubility and Traces of Hydrates. *J. Phys. Chem. C* **2014**, *118* (9), 4860−4868.

(46) Luzar, A.; Bratko, D. Gas Solubility in Hydrophobic Confinement. *J. Phys. Chem. B* **2005**, *109* (47), 22545−22552.

(47) Li, W.; Nan, Y.; Zhang, Z.; You, Q.; Jin, Z. Hydrophilicity/Hydrophobicity Driven Co2 Solubility in Kaolinite Nanopores in Relation to Carbon Sequestration. *Chem. Eng. J.* **2020**, *398*, 125449.

(48) Apostolopoulou, M.; Santos, M. S.; Hamza, M.; Bui, T.; Economou, I. G.; Stamatakis, M.; Striolo, A. Quantifying Pore Width Effects on Diffusivity Via a Novel 3d Stochastic Approach with Input from Atomistic Molecular Dynamics Simulations. *J. Chem. Theory Comput.* **2019**, *15* (12), 6907−6922.

(49) Apostolopoulou, M.; Stamatakis, M.; Striolo, A.; Dusterhoft, R.; Hull, R.; Day, R. A Novel Modeling Approach to Stochastically Evaluate the Impact of Pore Network Geometry, Chemistry and Topology on Fluid Transport. *Transport in Porous Media* **2021**, *136* (2), 495−520.

(50) Ho, L. N.; Clauzier, S.; Schuurman, Y.; Farrusseng, D.; Coasne, B. Gas Uptake in Solvents Confined in Mesopores: Adsorption Versus Enhanced Solubility. *J. Phys. Chem. Lett.* **2013**, *4* (14), 2274−2278.

(51) Andoh, Y.; Yoshii, N.; Yamada, A.; Fujimoto, K.; Kojima, H.; Mizutani, K.; Nakagawa, A.; Nomoto, A.; Okazaki, S. All-Atom Molecular Dynamics Calculation Study of Entire Poliovirus Empty Capsids in Solution. *J. Chem. Phys.* **2014**, *141* (16), 165101.

(52) Pollack, G. L. Why Gases Dissolve in Liquids. *Science* **1991**, *251* (4999), 1323−1330.

(53) Israelachvili, J. N. *Intermolecular and Surface Forces*; Academic press, 2011.

(54) Ho, T. A.; Ilgen, A. Density Fluctuation in Aqueous Solutions and Molecular Origin of Salting-out Effect for Co2. *J. Phys. Chem. B* **2017**, *121* (51), 11485−11491.

(55) Hillyer, M. B.; Gibb, B. C. Molecular Shape and the Hydrophobic Effect. *Annu. Rev. Phys. Chem.* **2016**, *67*, 307−329.

(56) Ball, P. Water as an Active Constituent in Cell Biology. *Chem. Rev.* **2008**, *108* (1), 74−108.

(57) Rego, N. B.; Patel, A. J. Understanding Hydrophobic Effects: Insights from Water Density Fluctuations. *Annual Review of Condensed Matter Physics* **2022**, *13*, 303−324.

(58) Hummer, G.; Garde, S.; García, A. E.; Pohorille, A.; Pratt, L. R. An Information Theory Model of Hydrophobic Interactions. *Proc. Natl. Acad. Sci. U. S. A.* **1996**, *93* (17), 8951−8955.

(59) Godawat, R.; Jamadagni, S. N.; Garde, S. Characterizing Hydrophobicity of Interfaces by Using Cavity Formation, Solute Binding, and Water Correlations. *Proc. Natl. Acad. Sci. U. S. A.* **2009**, *106* (36), 15119−15124.

(60) Jamadagni, S. N.; Godawat, R.; Garde, S. Hydrophobicity of Proteins and Interfaces: Insights from Density Fluctuations. *Annu. Rev. Chem. Biomol. Eng.* **2011**, *2*, 147−171.

(61) Maginn, E. J.; Messerly, R. A.; Carlson, D. J.; Roe, D. R.; Elliot, J. R. Best Practices for Computing Transport Properties 1. Self-Diffusivity and Viscosity from Equilibrium Molecular Dynamics

[Article V1.0]. *Living Journal of Computational Molecular Science* **2020**, *2* (1), 6324.

(62) Tsimpanogiannis, I. N.; Maity, S.; Celebi, A. T.; Moultos, O. A. Engineering Model for Predicting the Intradiffusion Coefficients of Hydrogen and Oxygen in Vapor, Liquid, and Supercritical Water Based on Molecular Dynamics Simulations. *Journal of Chemical & Engineering Data* **2021**, *66* (8), 3226−3244.

(63) Krynicki, K.; Green, C. D.; Sawyer, D. W. Pressure and Temperature Dependence of Self-Diffusion in Water. *Faraday Discuss. Chem. Soc.* **1978**, *66* (0), 199−208.

(64) Le, T. T. B.; Striolo, A.; Gautam, S. S.; Cole, D. R. Propane−Water Mixtures Confined within Cylindrical Silica Nanopores: Structural and Dynamical Properties Probed by Molecular Dynamics. *Langmuir* **2017**, *33* (42), 11310−11320.

(65) Siboulet, B.; Molina, J.; Coasne, B.; Turq, P.; Dufreche, J. F. Water Self-Diffusion at the Surface of Silica Glasses: Effect of Hydrophilic to Hydrophobic Transition. *Mol. Phys.* **2013**, *111* (22−23), 3410−3417.

(66) Liu, Y.-C.; Wang, Q.; Lu, L.-H. Water Confined in Nanopores: Its Molecular Distribution and Diffusion at Lower Density. *Chem. Phys. Lett.* **2003**, *381* (1), 210−215.

(67) Corral-Casas, C.; Gibelli, L.; Borg, M. K.; Li, J.; Al-Afnan, S. F. K.; Zhang, Y. Self-Diffusivity of Dense Confined Fluids. *Phys. Fluids* **2021**, *33* (8), 082009.

(68) Farmahini, A. H.; Bhatia, S. K. Differences in the Adsorption and Diffusion Behaviour of Water and Non-Polar Gases in Nanoporous Carbon: Role of Cooperative Effects of Pore Confinement and Hydrogen Bonding. *Mol. Simul.* **2015**, *41* (5−6), 432−445.

(69) Oliver, M. C.; Zheng, R.; Huang, L.; Mehana, M. Molecular Simulations of Hydrogen Diffusion in Underground Porous Media: Implications for Storage under Varying Pressure, Confinement, and Surface Chemistry Conditions. *Int. J. Hydrogen Energy* **2024**, *65*, 540−547.

(70) Liu, P.; Harder, E.; Berne, B. J. On the Calculation of Diffusion Coefficients in Confined Fluids and Interfaces with an Application to the Liquid−Vapor Interface of Water. *J. Phys. Chem. B* **2004**, *108* (21), 6595−6602.

(71) Argyris, D.; Cole, D. R.; Striolo, A. Dynamic Behavior of Interfacial Water at the Silica Surface. *J. Phys. Chem. C* **2009**, *113* (45), 19591−19600.

(72) Mutisya, S. M.; Kirch, A.; de Almeida, J. M.; Sanchez, V. M.; Miranda, C. R. Molecular Dynamics Simulations of Water Confined in Calcite Slit Pores: An NMR Spin Relaxation and Hydrogen Bond Analysis. *J. Phys. Chem. C* **2017**, *121*, 6674.

(73) Thompson, A. P.; Aktulga, H. M.; Berger, R.; Bolintineanu, D. S.; Brown, W. M.; Crozier, P. S.; in 't Veld, P. J.; Kohlmeyer, A.; Moore, S. G.; Nguyen, T. D.; et al. Lammps - a Flexible Simulation Tool for Particle-Based Materials Modeling at the Atomic, Meso, and Continuum Scales. *Comput. Phys. Commun.* **2022**, *271*, 108171.

(74) Verlet, L. Computer "Experiments" on Classical Fluids. I. Thermodynamical Properties of Lennard-Jones Molecules. *Phys. Rev.* **1967**, *159* (1), 98−103.

(75) Nosé, S. A Molecular Dynamics Method for Simulations in the Canonical Ensemble. *Mol. Phys.* **1984**, *52* (2), 255−268.

(76) Hoover, W. G. Canonical Dynamics: Equilibrium Phase-Space Distributions. *Phys. Rev. A* **1985**, *31* (3), 1695−1697.

(77) Parrinello, M.; Rahman, A. Polymorphic Transitions in Single Crystals: A New Molecular Dynamics Method. *J. Appl. Phys.* **1981**, *52* (12), 7182−7190.

(78) Ryckaert, J.-P.; Ciccotti, G.; Berendsen, H. J. C. Numerical Integration of the Cartesian Equations of Motion of a System with Constraints: Molecular Dynamics of N-Alkanes. *J. Comput. Phys.* **1977**, *23* (3), 327−341.

(79) Linstrom, P. J.; Mallard, W. G. The Nist Chemistry Webbook: A Chemical Data Resource on the Internet. *Journal of Chemical & Engineering Data* **2001**, *46* (5), 1059−1063.

(80) Cygan, R. T.; Liang, J.-J.; Kalinichev, A. G. Molecular Models of Hydroxide, Oxyhydroxide, and Clay Phases and the Development of a General Force Field. *J. Phys. Chem. B* **2004**, *108* (4), 1255−1266.

(81) Berendsen, H. J. C.; Grigera, J. R.; Straatsma, T. P. The Missing Term in Effective Pair Potentials. *J. Phys. Chem.* **1987**, *91* (24), 6269−6271.

(82) Pouvreau, M.; Greathouse, J. A.; Cygan, R. T.; Kalinichev, A. G. Structure of Hydrated Kaolinite Edge Surfaces: Dft Results and Further Development of the Clayff Classical Force Field with Metal−O−H Angle Bending Terms. *J. Phys. Chem. C* **2019**, *123* (18), 11628−11638.

(83) Buch, V. Path Integral Simulations of Mixed Para-D2 and Ortho-D2 Clusters: The Orientational Effects. *J. Chem. Phys.* **1994**, *100* (10), 7610−7629.

(84) Köster, A.; Thol, M.; Vrabec, J. Molecular Models for the Hydrogen Age: Hydrogen, Nitrogen, Oxygen, Argon, and Water. *Journal of Chemical & Engineering Data* **2018**, *63* (2), 305−320.

(85) Hirschfelder, J. O.; Curtiss, C. F.; Bird, R. B.. *The Molecular Theory of Gases and Liquids*; John Wiley & Sons, 1964.

(86) Yang, Q.; Zhong, C. Molecular Simulation of Adsorption and Diffusion of Hydrogen in Metal−Organic Frameworks. *J. Phys. Chem. B* **2005**, *109* (24), 11862−11864.

(87) Marx, D.; Nielaba, P. Path-Integral Monte Carlo Techniques for Rotational Motion in Two Dimensions: Quenched, Annealed, and No-Spin Quantum-Statistical Averages. *Phys. Rev. A* **1992**, *45* (12), 8968−8971.

(88) Bouanich, J. P. Site-Site Lennard-Jones Potential Parameters for N2, O2, H2, Co and Co2. *Journal of Quantitative Spectroscopy and Radiative Transfer* **1992**, *47* (4), 243−250.

(89) Sun, Y.; DeJaco, R. F.; Li, Z.; Tang, D.; Glante, S.; Sholl, D. S.; Colina, C. M.; Snurr, R. Q.; Thommes, M.; Hartmann, M. Fingerprinting Diverse Nanoporous Materials for Optimal Hydrogen Storage Conditions Using Meta-Learning. *Science Advances* **2021**, DOI: 10.1126/sciadv.abg3983.

(90) Belof, J. L.; Stern, A. C.; Space, B. An Accurate and Transferable Intermolecular Diatomic Hydrogen Potential for Condensed Phase Simulation. *J. Chem. Theory Comput.* **2008**, *4* (8), 1332−1337.

(91) Belof, J. L.; Stern, A. C.; Space, B. A Predictive Model of Hydrogen Sorption for Metal−Organic Materials. *J. Phys. Chem. C* **2009**, *113* (21), 9316−9320.

(92) Ali, A.; Cole, D. R.; Striolo, A. Cushion Gas Effects on Clay-Hydrogen-Brine Wettability at Conditions Relevant to Underground Gas Storage. *Int. J. Hydrogen Energy* **2024**, *58*, 668−677.

(93) Barraco, M.; Neyertz, S.; Benes, N. E.; Brown, D. Comparison of Eight Classical Lennard-Jones-Based H2Molecular Models in the Gas Phase at Temperatures and Pressures Relevant to Hydrogen on-Board Storage Tanks. *J. Phys. Chem. A* **2023**, *127* (30), 6335−6346.

https://doi.org/10.1021/acs.jpclett.4c01684
J. Phys. Chem. Lett. XXXX, XXX, XXX−XXX